Journal of Materials Chemistry B

Shape Memory Materials for Electrically-Powered Soft Machines

Journal:	*Journal of Materials Chemistry B*
Manuscript ID	TB-REV-02-2020-000392.R1
Article Type:	Review Article
Date Submitted by the Author:	11-Apr-2020
Complete List of Authors:	Huang, Xiaonan; Carnegie Mellon University, Mechanical Engineering Michael, Ford; Carnegie Mellon University Patterson, Zachary; Carnegie Mellon University Zarepoor, Masoud; Lake Superior State University Pan, Chengfeng; Carnegie Mellon University, Mechanical Engineering Majidi, Carmel; Carnegie Mellon University, Mechanical Engineering

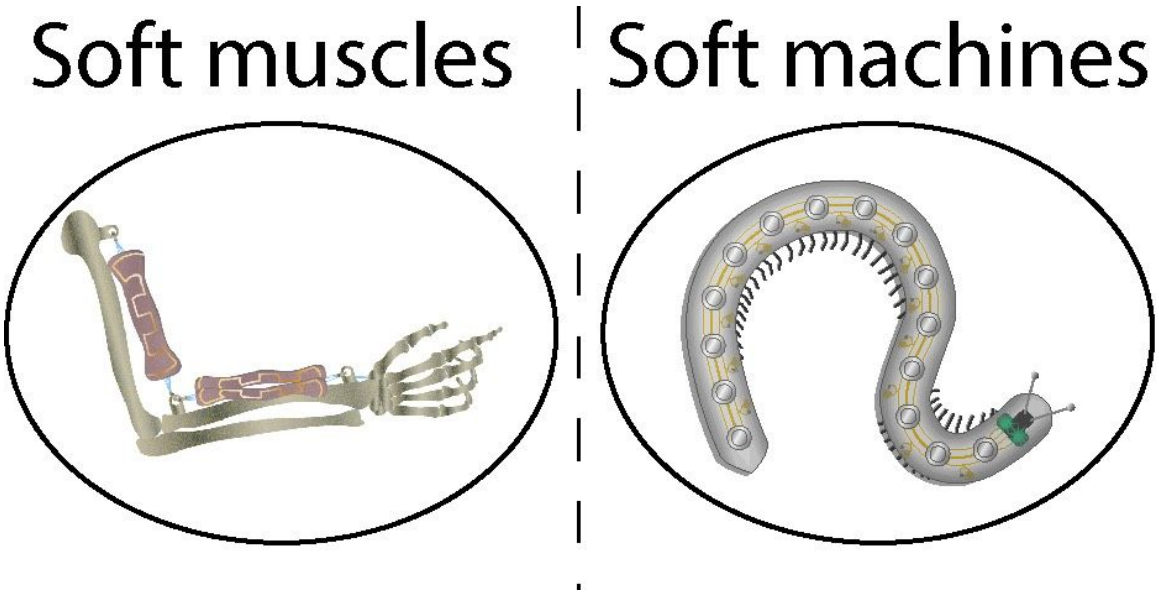

We review the recent progress of electrically-powered artificial muscles and soft machines using shape memory alloy and liquid crystal elastomer.

ARTICLE

Shape Memory Materials for Electrically-Powered Soft Machines

Xiaonan Huang,[a] Michael Ford,[a] Zach J. Patterson,[a] Masoud Zarepoor,[a,b] Chengfeng Pan,[a] and Carmel Majidi *[a]

-Received 00th January 20xx,
Accepted 00th January 20xx

DOI: 10.1039/x0xx00000x

Soft robots represent an emerging class of biologically-inspired machines that are primarily composed of elastomers, fluids, and other forms of soft matter. Current examples include crawling and swimming robots that exhibit the mobility, mechanical compliance, and deformability of various classes of soft biological organisms, ranging from cephalopods and larvae to marine fish and reptiles. Rather than using electrical motors, soft robots are powered with "artificial muscle" actuators that change shape and stiffness in response to controlled stimulation. In recent years, conductive shape memory materials have become especially popular for soft robot actuation due to the ability to stimulate these materials with on-board microelectronics and miniature batteries. Here, we will review recent progress in the development of artificial muscle using shape memory materials that can be stimulated through electrical activation. This includes the use of shape memory alloy (SMA) to create fully untethered soft robots capable of biologically-relevant locomotion speeds as well as recent progress in engineering liquid crystal elastomer (LCE) composites that are capable of robust electrically-powered actuation.

1 Introduction

Soft robotics is a highly interdisciplinary field that combines traditional practices in robotics and computer science with the principles and practices from the life sciences, materials engineering, and chemistry[1–4]. Unlike conventional machines and robotic hardware, soft robots are primarily composed of elastomers, fluids, and other forms of soft matter. Their composition enables them to mechanically deform and physically interact with objects without imposing large stress concentrations. While originally focused on pneumatic "artificial muscle" actuators for human motor assistance[5] and tentacle-like continuum end effectors for robotic manipulation[6] , the field has since expanded to include a wide variety of biologically-inspired robots with a rich range of material architectures, functionalities, and applications.

In addition to pneumatic actuators, soft robots can also be powered using electrostatics, electromagnetism, combustion, and natural muscle tissue[7]. The advantage of these techniques over pneumatic artificial muscles is that they eliminate the need for pumps, valves, or compressed air sources that may add bulk and weight to the robot. Another popular method for artificial muscle actuation is to use electrically responsive shape memory materials such as shape memory alloys (SMAs), shape memory polymers (SMPs), and liquid crystal elastomer (LCEs). These materials undergo a phase change that can alter their stiffness and/or natural (unstressed) rest shape. Details of this process are described below in **Sec. 2.1** for representative classes of shape memory materials. While there are other types of soft materials that change shape in response to electrical stimulation, such as dielectric elastomer actuators and electro-responsive hydrogels, such materials do not share the same programmable shape memory properties as described here.

Among the various types of shape memory materials currently used in soft robotics, SMA actuation is particularly attractive since the alloy can be activated electrically with Joule (Ohmic) heating. That is, the actuator can undergo thermal activation by directly passing electrical current through the material. The electrical resistance of the material generates heat, which, in the case of SMA, induces a phase change from a highly compliant and malleable Martensite crystal phase to a highly stiff and shape-restoring Austenite phase[8]. In contrast, LCEs are electrically insulating and cannot support the current necessary for Joule heating. Instead, actuation is activated by heating through the phase transition of the liquid crystal using an external heat source (e.g. heat gun, hot plate), a Joule heating element, or conductive fillers or by disrupting the liquid crystal ordering through some other stimulus like light[9–12]. In recent years, there has been progress in engineering LCE composites that are conductive and can be activated electrically. As described below in Sec. 2.1.2, electrically conductive LCEs are achieved by embedding the elastomer with a percolating network of conductive particles such as carbon powder or microdroplets of liquid-phase metal alloy.

In this highlight, we will review progress in the development of artificial muscles using shape memory materials that can be stimulated through electrical signal. This overview will include a survey of the materials and their response as well as a description of artificial muscle architectures based on shape memory materials and their applications in soft robotics. We will primarily focus on recent advancements since 2017 related to the use of SMAs and electrically conductive composites of

[a] Soft Machines Lab; Carnegie Mellon University; Pittsburgh, Pennsylvania USA.
[b] Mechanical Engineering; Lake Superior State University; Sault Sainte Marie, Michigan USA..
† Author for correspondence: cmajidi@andrew.cmu.edu, +1 412 268 2492

LCEs. For a more complete review of soft robotic actuation, including prior work on SMAs, LCEs, as well as other soft material architectures like pneumatic actuators, dielectric elastomer actuators, conducting polymer actuators, shape memory polymers, piezoelectric actuators and hydrogel actuators, the interested reader should refer to review papers by Hines et al.[13], Rich et al.[7], Zhao et al.[14], Liu et al.[15], Chopra et al[16] and Erol et al.[17].

2 Artificial Muscles based on Shape Memory Materials

Drawing inspiration from natural muscle, "artificial muscles" are typically designed to change both their shape and stiffness in response to controlled stimulation. With SMAs and LCEs, shape change is often accomplished with a thermally induced change in crystal structure or a transition between an amorphous and ordered molecular state. In this section, we review the composition, material properties, and thermal responses of SMAs and LCEs and describe how they are incorporated into "artificial muscle" actuators for applications in soft robotics. This section includes discussion on the interplay between crystal structure or molecular ordering with bulk mechanical properties and shape memory effects.

Referring to **Fig. 1**, one embodiment of "shape memory" that is common to SMAs and LCEs is the ability of a material that is malleable and deforms inelastically under mechanical loading (e.g., to a length *L'*) to spontaneously recover its natural rest state (e.g., length L_0). For example, in the presence of a fixed external tensile load *F*, this transition will cause a strip of material to contract to a final length

$$L = \left\{1 + \frac{F}{EA}\right\} L_0 < L', \quad (1)$$

where A is the original cross-sectional area of the strip. In the case of SMA, the material will also exhibit a change in stiffness (i.e. elastic modulus *E*) as it undergoes this transition.

2.1 Shape Memory Materials in Soft Robotics

2.1.1 Shape Memory Alloy

SMAs are a group of alloys that exhibit a reversible change in both shape and rigidity when thermally stimulated. Common SMAs include Fe-based, Cu-based and Ni-Ti-based alloys (Nitinol). Among these, Ni-Ti-based SMAs are more popular and have been commercialized because of their greater thermal stability, recoverable strain, and corrosion resistance compared to other SMA compositions[8]. In this paper, we mainly focus on Nitinol although other SMA compositions, such as alloys containing Fe or Cu, have distinct advantages (e.g. ultra-low fatigue[18,19]) and have been utilized in applications like concrete reinforcement[20,21] and strain sensors[22].

The shape memory effect in SMAs is associated with a first-order displacive martensitic phase transformation. SMAs transform between the monoclinic martensite phase and cubic austenite phase when heated and cooled. Depending on the amount of pre-strain, this phase change can result in a contractile strain of 4-8%[7,8,23]. Nitinols are relatively soft and malleable at the martensite phase

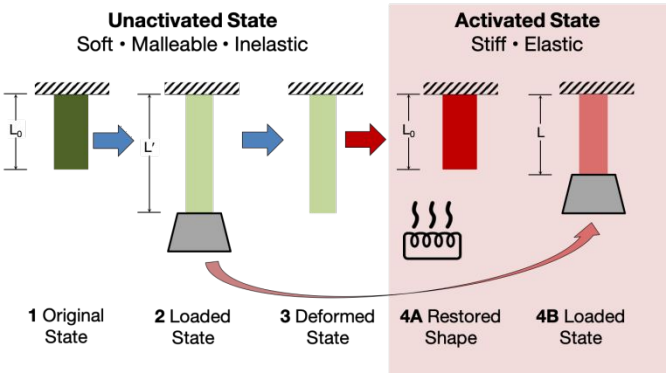

Fig. 1 While unactivated, SMA and LCE-based shape memory materials plastically deform in response to a load (1-3). When activated, the material restores its original state in absence of load (4A), or partially recovers its original state in the presence of a load (4B).

(Young's modulus: ~28-41 GPa) and transform into a hard and rigid austenite phase (Young's modulus: ~82-100 GPa) when heated beyond a threshold temperature. There are two types of crystal structures in the martensite phase – twinned and detwinned. The detwinning process can be induced by stress during which the atomic plane rearranges without slipping. For this reason, Nitinol is malleable while in the martensite phase.

There are four key temperature values that define the start and finish temperature for the reversible phase transition: (A_s) austenite start temperature; (A_f) austenite finish temperature; (M_s) martensite start temperature; and (M_f) martensite finish temperature. The phase transformation is associated with significant nonlinear thermal hysteresis, which leads to a low energy efficiency (~3%)[8].

Shape memory in SMAs can be categorized as either a one-way shape memory effect (OWSME) or a two-way shape memory effect (TWSME). For the OWSME, after it is deformed in the martensite phase, the SMA can return to its original shape after it is heated above A_f. It then keeps this shape after cooling below M_f (absent an applied load). For the TWSME, the SMA can "memorize" a unique shape for each of these phases (martensite and austenite) and reversibly switch between these two shapes when heated and cooled.

While thermal stimulation is most commonly used to trigger phase transformation, Nitinol also exhibits pseudoelasticity, where the material can switch between austenite and martensite phases when subjected to a mechanical load between A_f and M_d (martensite deformation temperature). In this way, pseudoelasticity allows Nitinol to function like a spring that recovers its original shape once external load is removed. This property of Nitinol is typically exploited in actuators with antagonistic architectures, which have been utilized in soft robotics[24,25] and medical application[26].

Although Nitinol has been commercialized for decades and widely applied in soft robotics, its relatively high Young's modulus can make it challenging to use in applications that require high mechanical compliance. For these applications, LCEs can be more promising since they remain relatively compliant in both their natural and activated states.

2.1.2 Liquid Crystal Elastomer

LCEs represent a class of shape memory materials that have attracted increasing interest in the field of soft robotics. Advantages of LCEs relative to Nitinol include high mechanical compliance (typically < 10 MPa), high actuation strain (50-400%)[27–29], controllable processability[27,30–32], tunability of the chemical structure[33], and the option for arbitrary shape transformations (e.g., from flat sheets to complex 3D shapes). However, limitations of LCEs compared to Nitinol include lower work density, the lack of significant stiffness change during actuation, poor thermal conductivity, and the inability to induce shape memory through electrical Joule heating.

LCEs are networks of liquid crystal mesogens connected by flexible spacers and crosslinkers[10]. The liquid crystal mesogens distinguish LCEs from other shape memory polymers, which may also find use as artificial muscles[14]. For LCEs, to function as an artificial muscle, the liquid crystal mesogens must be macroscopically ordered (e.g., by stretching uniaxially to form a *monodomain* with uniaxial order.) Disruption of the liquid crystal ordering will result in actuation. For example, the phase transition of the liquid crystal mesogens can drive actuation. When the material is heated above the phase transition of the liquid crystal mesogens, they become disordered. For a uniaxially-ordered LCE, heating will cause the LCE to contract along the direction of ordering.

Various combinations of liquid crystal, spacer, and crosslinker units[34,35] have been synthesized to control compliance, deformability, processability, actuation characteristics, and stimuli-responsiveness. Importantly, the liquid crystal ordering may or may not be directed during processing. For example, surface templating or shear extrusion can direct orientation to form unique shapes that exhibit a shape memory effect that is similar to TWSME in SMAs[27,36] and shape memory polymers[37]. If orientation is not controlled, the liquid crystal domains will form microscopic grains that are macroscopically disordered, i.e., a *polydomain*. The LCE must be subjected to an external mechanical load to induce the shape memory effect within polydomain samples. Otherwise, the shape will persist in the absence of a load based on the orientation of the liquid crystal domains.

For these compositions, LCEs are not thermally or electrically conductive. LCEs can be synthesized or processed to respond to light, which is useful for some robotic-like applications. However, light-controlled activation is not always practical in robotics applications, especially for structures with thicknesses that are greater than a few hundred micrometres and environments where ambient light may interfere with reversible actuation. LCEs have also been used as the dielectric layer for dielectric elastomer actuators to achieve fast actuation and directed shape programming[38]. Liquid crystal mesogens can align when subjected to an electric field; however, these embodiments of soft actuators require relatively large electric fields (on the order of 10^6 V m^{-1})[13,39–41].

Other approaches toward electrically activated LCEs have used surface heating elements[42,43] and/or conductive fillers. However, there is often a trade-off between deformability and electrical/thermal conductivity since the incorporation of rigid heating elements or conductive filler particles can restrict deformation. In addition, rigid elements can cause cracking or delamination during actuation. Examples of rigid conductive materials that can be embedded in LCE for heating include carbon black, carbon nanotubes, and metallic traces. Early research acknowledged the need for compliant heaters for LCEs, and one strategy to reduce mechanical mismatch between the heater and LCE was to use conductive polymer traces[44]. In general, replacing rigid heating elements with conductive materials that are soft and deformable would allow the actuator to operate without impairing the intrinsic shape memory properties of the LCE[45].

2.2 Artificial Muscle Architectures

Shape memory materials that can be directly actuated using electrical current require minimum auxiliary equipment and thus pave a pathway to achieve fully untethered soft robotic systems. In this section, we review the existing ways in which SMA and LCE based actuators have been designed and applied in soft robotic systems over the past few years.

2.2.1 Shape Memory Alloy Actuators

SMAs are a popular choice for soft actuation since they have a high work density (10^4-10^5 KJ/m^3), high force-to-weight ratio (~100), and fast actuation response (<1s)[7]. However, similar to other thermally-driven actuators, SMA actuators suffer from relatively low actuation bandwidth (0.5-5Hz)[7,46] and energy efficiency (~3%)[8]. This is due to the time required for the SMA to passively cool down at the end of each actuation cycle and the wasted energy from heat loss during both activation and cooling. To improve this, methods like embedding SMA wire inside thermally conductive elastomer have been used, as discussed below.

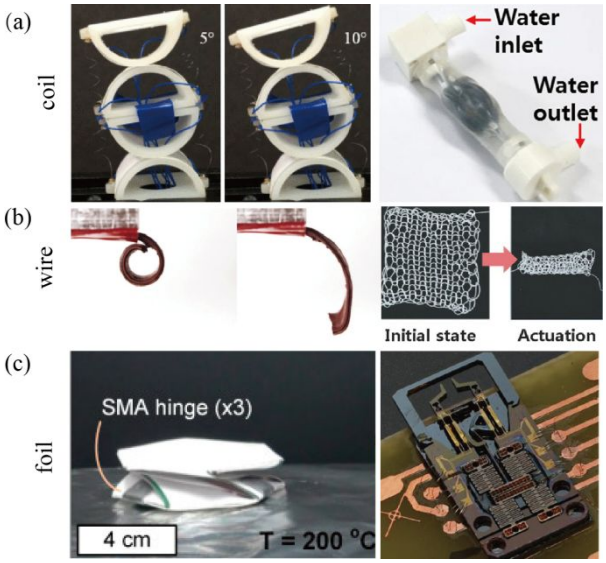

Fig. 2 Soft SMA actuators in the forms of coil, wire and foil. (a)SMA coil actuators with multiple SMA coils externally connected to origami joints (left) and active cooling (right). (Reproduced with permission [47] and [55], 2019, IEEE); (b) SMA wire actuators with SMA wire embeded in thermally conductive elastomer with a prestretched layer (left) and knitted with nylon wires (right) (Reproduced with permission [57], 2019, Wiley and [71], 2017 Wiley); (c) SMA foil actuators with SMA foils in kirigami structure (left) and in MEMS (right) (Reproduced with permission [77], 2018, Elsevier and [78], 2019, IEEE).

Soft actuators powered with SMAs are typically composed of elastomers embedded with Nitinol coil, wire, or foil. SMA coils are typically implemented as linear actuation components that are incorporated in robotic joints[47–50] or embedded in deployable mechanisms (e.g. origami structure)[51–53]. When attached to a hinge or joint, they can induce large rotations and torques due to their high strain (~200-1600%)[54] and force output[8]. Multiple SMA coils can be utilized in the actuator and selectively actuated to achieve multi-degree of freedom (DOF) actuation[47–49] (Fig. 2(a))(left)). To reduce the deactivation period, SMA coils can be implemented in combination with an antagonistic mechanism (e.g. antagonistic spring)[47,48,50,52] or active cooling system[55] (Fig. 2(a))(right)).

A common way to create a soft SMA actuator with Nitinol wire is to embed it inside of a matrix material (e.g. elastomer)[56–65]. Due to the stiffness mismatch, the strain change caused by the phase change of the Nitinol leads to a deformation of the matrix. To improve the actuation frequency, researchers have embedded SMA wire inside elastomers with high thermal conductivity[56–58,66] (Fig. 2(b))(left)) or hydrogel[60] to improve the heat dissipation in the cooling process. Another technique that has been widely used to increase the bandwidth of SMA actuation is to introduce an antagonistic mechanism to restore the natural state of the actuator during deactivation[57,63,67–70]. One method presented recently[57,58,61,63] is to prestrain the SMA wire or the matrix since it can provide antagonistic force without introducing additional stiffness (Fig. 2b)(left)). To achieve multi-degree of freedom (DOF) actuation, multiple SMA wires are arranged inside of the matrix and selectively actuated[67]. Compared with a coil, an SMA wire generates significantly less strain (4-8%)[7,8,23]. To improve this, researchers have knitted SMA wire with other materials (e.g. nylon)[71–73] (Fig. 2(b))(right)), woven the wires[74], or twisted the wire[62] to increase the strain. Besides being implemented as actuators to control robotics joints[65,72,73] or grippers[60,63,69,70], soft actuators fabricated with SMA wire can also be utilized as robotics limbs for soft robots[56–59,61,75,76] and feedback sensing components in haptic device[64] due to their high force to weight ratio and silent actuation properties.

SMA foil is typically incorporated into origami or kirigami structures as an actuation hinge without significantly increasing the size of the structure[77]. Examples include the twisting kirigami structure shown in Fig. 2(c))(left) and the MEMS-based actuator system[78] shown in Fig. 2(c))(right). Typically, SMA foil is patterned with UV laser micromachining, which enables the creation of planar shapes with fine resolution and complex geometries.

Lastly, there has been exciting work in recent years that combines SMA actuators with other thermally-responsive materials. Yuen et al.[79] had created variable-stiffness actuators with SMA wrapped around a thermoplastic fiber to create a multifunctional robot fabric. In this implementation, styrene-ethylene/butylene-styrene (SEBS) and polyactic acid (PLA) were used for the thermoplastic core and shell. More recently, Liao et al.[80] demonstrated the ability to create a variable-stiffness actuator by embedding SMA wire in polycaprolactone (PCL). PCL is a thermoplastic with a moderate softening temperature that had been previously used for stiffness-tuning tendons in soft robotics[81]. Because of the difference in phase-transition temperatures, the SMA-PCL actuator could be engineered to initially soften before it undergoes shape-memory bending due to SMA activation.

2.2.2 Liquid Crystal Elastomer Actuators

The main advantages of LCEs as soft actuators (Fig. 3(a)) include large actuation strain (> 400 %), compliance, processability, and tunable chemistry that enable multiresponsivity and multifunctionality[28,82–86]. LCEs are not electrically conductive and thus require conductive heating elements or fillers for electrically activated actuation[87]. Actuation characteristics such as work density, actuation speed, and durability of LCE actuators are less often reported in current literature, although progress toward soft robotic applications will continue to reprioritize the importance of such metrics.

2.2.2.1 LCE Actuator Performance

Work density has been more commonly characterized for LCE actuators that are activated by ambient heating than those that are activated electrically. Values typically range from about 1 to 730 kJ/m^3, depending on the LCE chemistry and actuator architecture[28,36,88]. Recent progress on LCE molecular design achieved actuation stress and work density as high as 2.5 MPa and 1268 kJ/m^3, respectively, by synthesizing an interpenetrating polyurethane/polyacrylate LCE that was heated by ambient heating[89]. This work represents a significant step toward artificial muscles based on LCE actuators. For electrically activated LCE actuators, work densities of about 30-150 kJ/m^3 have been reported[45,90]. The additional materials used for Joule heating add volume and are inactive in actuation and thus would contribute detrimentally to work density. Otherwise, there is no reason to think that the work density for thermally activated LCE actuators could not be achieved by electrically activated LCE actuators, as long as heating of the actuator is uniform and controlled.

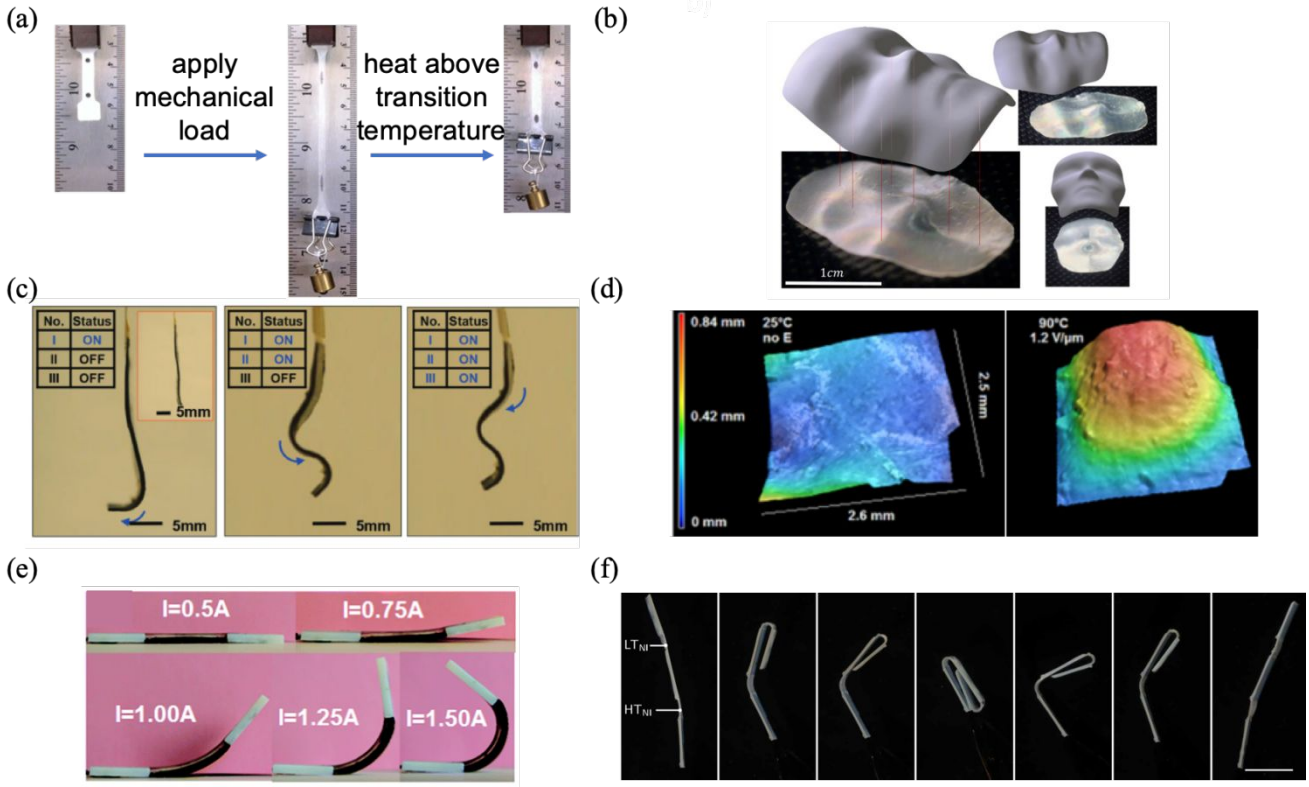

Fig. 3 LCE actuators are capable of large actuation strains. The example shown here is a polydomain sample that requires the application of a mechanical load for reversible actuation (a) (Reproduced with permission [86], 2016, JoVE). LCE actuators are capable of complex actuation like those with Gaussian curvature. Above the transition temperature (T_{NI}), the LCE takes a shape of face. The scale bar is 1 cm (b) (Reproduced with permission [95], 2019, NAS). Complex actuation can be achieved in LCEs by using multiple integrated heaters (c) (Reproduced with permission [105], 2018, Wiley). Fast actuation is possible with complex shape by using the electromechanical coupling of CNTs in CNT-LCE composites. A topological map was obtained with a Keyence optical profilometer (d) (Reproduced with permission [109], 2018, ACS). Bilayer and related structures produce bending actuation in LCEs (e) (Reproduced with permission [110], 2017, RSC), which can be used to fabricate complex bending structure (f) (Reproduced with permission [108], 2019, AAAS).

Actuation speeds for LCE actuators that are electrically activated have been limited by heating/cooling rather than any intrinsic molecular kinetics. Actuation speeds are often slow (< 0.1 Hz) due to slow heat transfer during Joule heating and cooling. There is substantial room for improvement in this area of LCE actuator research. For example, sharp phase transitions where small temperature changes result in large actuation strain could be leveraged for faster actuation. Active cooling or actuation in a convective fluid like water could improve actuation rates. Heat transfer also plays a role in energy efficiency, since the input energy during actuation can be lost to the ambient environment[91]. Joule-heated LCE actuation can be faster and more efficient by lowering the temperature of the phase transition, which is possible through molecular design[82]. Efforts to miniaturize LCE actuators also aid in faster actuation[92]. Faster actuation may be possible for actuation that is triggered by an electric field rather than electrical Joule heating. For example, fast bending actuation (3.5 s) was possible for LCEs that included an ionic liquid and were activated by an electric field[93]. The positive and negative ions were of dissimilar sizes, and the actuation was induced by the anisotropic distribution of ions under the applied field rather than the LC phase transition.

Research suggests that the actuation durability for LCE actuators is good relative to other thermal actuators like SMAs. Stability through hundreds or thousands of cycles is possible and has been demonstrated by several groups[44,45,94]. We showed that an electrically activated LCE could be subjected to 100,000 cycles at 2.5 % actuation strain[41]. In these cases, the sample did not fail mechanically nor electrically, and the failure mechanisms have yet to be explored in detail. A substantial constraint to test durability/failure is time, especially with slow ambient cooling. Our group and others have shown that LCE actuators can undergo cycling to larger strains (> 30 %) for thousands of cycles[44,45]. While the durability of LCE actuators is promising, further work to understand and optimize durability will be important for the future of this area of research.

Linear actuation is easily accomplished in monodomain or polydomain LCEs, if the LCE is subjected to an applied load. For polydomain LCEs, the applied load orients the director of the liquid crystal domains, and a destabilization of the liquid crystal order results in linear actuation. Another advantage of LCEs over SMAs is the capability for complex and/or arbitrary modes of actuation, like the transformation of a flat sheet to a cone with Gaussian curvature (Fig. 3(b))[36,95,96]. Until recently, the majority of LCE actuators were mostly limited to thin film architectures, either to accommodate responsivity to light or to comply with the constraints of the chemical synthesis and preparation of monodomain samples[36]. 3D LCE

architectures are also of interest for soft actuators[97–99]. LCE actuators were also processed as fibers[100,101]. With the development of simple "click" chemistries that use commercially available starting materials, other architectures that include tubular actuators and 3D-printed structures can be synthesized[30,85,90].

2.2.2.2 Electrically-Operated LCE Actuators

The most straightforward route to electrically activated LCE actuators is to use a conductive wire that is either atop an LCE or sandwiched between two LCE sheets[91,94]. Conductive wires are often patterned into serpentine structures to overcome limits of deformability[102]. Multiple wires can be used to separately heat discrete regions of a given structure to facilitate actuation that is highly predictable[102]. LCEs inherently have low thermal conductivity, and activation may be slow for these architectures. As is true for all cases where cooling is limited by convection of air, deactivation is also slow.

Carbon-based heating elements or inclusions remain a popular choice for Joule-heated actuation of LCEs. Compared to LCE actuators with embedded conductive wires, LCE composites with carbon-based inclusions have higher thermal conductivity and therefore faster heat dissipation than unfilled LCEs. Graphite was used in one of the first implementations of active LCE actuators[103]. Since then, researchers have explored processing of carbon black (CB) and carbon nanotubes (CNTs) in LCEs. Processing should be optimized to produce effective LCE actuators with carbon-based inclusions. High loadings of CB reduce linear actuation strain since the rigid filler imposes a mechanical constraint on the matrix. In addition, the mechanical mismatch of the rigid filler and soft matrix could result in delamination and loss of percolation of the conducting particles[104].

Wang et al. noted that carbon black at high weight content limited thermally induced contraction[105]. For example, previous reports showed that 2 wt. % CB dispersed in an LCE matrix reduced contractile strain from 35 % to 27.7 %. Percolation for appreciable electrical conductivity (ca. 0.01 S/cm) was not achieved until the CB-LCE composite contained 15 wt. % CB[44], which further reduced contractile strain to 5.2 %. By dispersing particles on the surface of the LCE, it's possible to balance actuation, electrical conductivity, and thermal conductivity. Therefore, Wang et al. aimed to use CB to improve thermal dissipation while Joule-heating with a patterned Au heater. However, at 2 wt. % CB, it is not clear that there is a substantial improvement in thermal conductivity[106]. Still, the architecture of the LCE and surface heaters facilitated predictable, complex shape-morphing. For example, by using an architecture with three separate heaters, a monolithic actuator formed multiple distinct structures upon Joule-heating (Fig. 3(c)).

As an alternative to CB, CNTs can also be used for Joule-heated actuation. One substantial challenge to form CNT composites is CNT processing and dispersion. To mitigate this challenge, Kim and co-workers adopted a sandwich structure of a thin LCE film between forest-drawn CNT sheets[107]. The CNT sheets were embedded near the top and bottom surfaces of the LCE and served as templating layers for LCE ordering while also increasing the elastic modulus. The authors used 1 or 5 layers on each side (about 0.1 and 0.5 wt. % respectively). As with CB, increasing CNT loading decreased reversible actuation strain for the LCE actuator, which underwent 35 % contractile strain with no CNT layers and 16 % contractile with 5 CNT layers. However, in contrast to what would be expected for other particle-filled LCE composites, the contractile blocking stress increased as CNT content increased (1.28 ± 0.12 MPa for the LCE with no CNT layers to 1.97 ± 0.05 MPa for 5 CNT layers). Another beneficial attribute of this architecture is the potential for multifunctional responsivity; the CNT-LCE exhibits a photothermal response and can bend toward a moderate light source (e.g., light from a mobile phone).

Another potential advantage for LCE actuators that are dispersed with CNTs relate to alternative mechanisms for actuation besides Joule heating. CNTs have highly anisotropic polarizability and dielectric constant. Consequently, CNTs under an applied electric field can impose a torque on the surrounding LCE matrix[108]. The imposed torque results in mechanical contraction without heating. Therefore, heat dissipation is not a concern, and fast actuation is more feasible in ambient conditions.

Guin et al. recently highlighted the advantage enabled by avoiding electrothermal stimulation, with shape recovery occurring over a period of less than 1 s for an LCE actuator with 0.02 wt. % single-walled CNTs[109] (Fig. 3(d)). Single-walled CNTs were dispersed in the LCE before curing using a photoalignment layer that could produce complex and arbitrary shapes. The researchers posited that rotational torque of the CNTs could not be solely responsible for the 18% linear contraction observed and proposed that interfacial charge accumulation produced an electrostrictive force that contributed to actuation under the applied field. Complex shape morphing from a flat sheet to a curved surface was also possible, which could be important for complex actuation in soft robotics. However, thermally induced contraction of the LCE was reduced from 140 % to 60 % when CNTs were added, and high electric fields (e.g., > 1×10^6 V/m) along with elevated temperatures were necessary to trigger LCE actuation[87]. The reduction of thermally induced contraction and the elevated temperatures needed for actuation might not be persistent with optimization of the LCE chemistry and composite fabrication. CNTs have been previously used for electromechanical LCE actuators without these disadvantages[108]. Nonetheless, the work highlights an advantage of electromechanical actuation over electrothermal actuation since heating and cooling occurred rapidly (< 1 s).

2.2.2.3 Bilayer LCE Actuators

Some embodiments of LCE actuators take advantage of a rigid surface heating element or passive film atop the LCE to fabricate bilayer actuators. The bilayer structure places a constraint on linear actuation and enables bending or folding modes of actuation. In one recent implementation, Xiao et al. formed a bilayer actuator with a polyimide film as the constraining layer and used conductive wires to trigger actuation[94]. The actuator was a reprogrammable liquid crystal network, where heating and subsequent cooling in a certain orientation could reprogram reversible shape-morphing. Bending and helical coiling/uncoiling were possible. Helical coiling and uncoiling could potentially be used for rotational motion, which has been relatively underexplored compared to soft actuators with linear motion. Moreover, it could be used to exert a significant pushing

force, which is difficult for soft, thin film architectures. These features may warrant further studies. By selectively programming discrete sections of an actuator while also selectively placing the polyimide film on different sides of the actuator, bending and unbending with greater complexity was also achieved. For future studies, the use of a reprogrammable network is interesting and could be useful for applications where reconfigurable actuation is desired. However, a reprogrammable network may not be strictly necessary if other synthetic procedures or mechanical properties are more desirable. For example, direct shape-programming could be achieved by programming with a commonly used double-network[96].

Multimaterial processing permits the fabrication of complex structures that are similar to bilayer actuators with hinges as the basic building block for the structures[102,110] (Fig. 3(e)). Using LCE actuators that are adhered to 3D printed substrates, Yuan et al. fabricated complex structures like a periodic miura-ori structure that folds from a flat sheet to a sheet with ridges and valleys[110]. The structure was activated by 1.5A and required 3 min to reach a bending angle of 60°. Since the LCE is adhered to the substrate, delamination is possible with overheating, which limited actuation rate. Roach et al. later developed an LCE ink with a nematic to isotropic transition temperature of 42 °C, making it amenable to printing at room temperature, reducing chances of delamination, and reducing input power needed for actuation[111]. Selective control of Joule heating permits sequential folding of a box. Molecular design and 4D printing of LCEs have enabled similarly complex folding structures that are heated with ambient heating[112] (Fig. 3(f)).

2.2.2.4 LCE Actuators with Liquid Metal

Since rigid fillers and heating can restrict actuation, we recently explored deformable fillers for Joule heated actuation. Specifically, we introduced an LCE composite that used an alloy of gallium and indium[45]. The alloy is liquid at room temperature and can be easily dispersed as microparticles by shearing the liquid metal in the uncured LCE precursor. After curing, the composite can have high thermal and electrical conductivity, enabling Joule heated actuation. Both the unfilled LCE and the liquid metal LCE composite displayed reversible linear actuation with actuation strains > 50 %, suggesting that the deformability of the liquid metal is critical to retaining shape morphing characteristics while also permitting conductivity. Complex shape-programming for reversible shape morphing with Gaussian curvature was also demonstrated for the composite. Multifunctional actuators that use LCEs with liquid metal could have potential for integrated soft actuation and stretchable electronics in soft robotics applications.

3 Soft Robots Powered with Shape Memory Materials

Electrically powered actuators that incorporate shape memory materials have been used in recent years to create soft robots capable of crawling, walking, climbing, rolling, jumping and swimming. Because these actuators can be powered with small and lightweight batteries, it is possible to create fully untethered soft robots in which all the supporting power and electronics are located on-board. In this section, we review several recent implementations of tethered and untethered soft robots that are powered with electrically activated shape memory materials. Some of these implementations satisfy the formal definition of a robot in the sense that they contain an on-board microcontroller and can be programmed to execute various locomotion gaits. However, others are "robots" in the broader sense that they are capable of crawling or swimming motions but rely on an external power supply and signal generator to stimulate motion.

3.1 SMA-Powered Robots

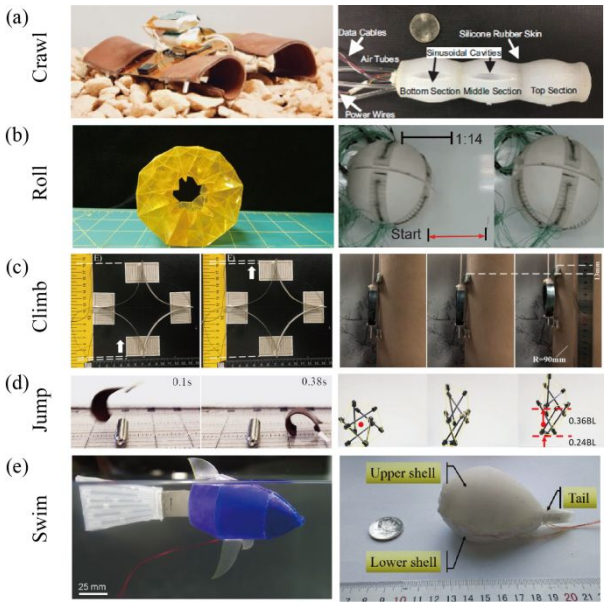

Fig. 4 Implementation of soft SMA actuators into soft robotic systems with locomotion modes of crawling, climbing, rolling, jumping and swimming. (a) Soft SMA crawling robots with untethered reptile-like (left) and worm-like (right) crawling locomotion (Reproduced with permission [61], 2018, AAAS and [123], 2017, IEEE); (b) Soft SMA rolling robots with geometry change (left) and propulsion mechanism (right) leading to rolling locomotion (Reproduced with permission [120], 2019, Elsevier and [117], 2019, Springer); (c) Soft SMA climbing robots with electrostatic (left) and microspine array (right) adhesion mechanism (Reproduced with permission [127] and [129], 2019, IEEE); (d) Soft SMA jumping robots with prestrained SMA wire (left) and SMA spring (right) (Reproduced with permission [57], 2019, Wiley and [125], 2019, ACS); (e) Soft SMA swimming robots with SMA actuators as caudal fin (left) and a valve to control the water volume in the swimmer (right) leading to a forward locomotion (Reproduced with permission [56], 2017, NAS, and [132], 2017, IEEE).

SMAs have been implemented into soft robotic systems as the actuation source for decades thanks to their unique combination of material and functional properties. These properties include high work density, high force-weight ratio, shape programmability, electrical activation capability, low power requirements, fast change between soft and rigid phases, large and reversible deformation, silent activation, and high resistance to mechanical impact[7,8,23,54,113–115]. Despite these advantages, the majority of SMA-driven robots are tethered since untethered robotic architectures require careful selection of materials for body architecture and miniaturized

Journal of Materials Chemistry B Journal of Materials Chemistry B

electronics for power and control along with a tight system-level integration of actuators, body architecture and electronics. In this section, we review recent studies of both tethered and untethered SMA-driven robots by various locomotion modes, including crawling, climbing, rolling, jumping and swimming.

One type of SMA-driven soft crawling robot involves reptile-like motion, which requires the SMA actuators to serve as load-bearing limbs to hold the weight of the body and on-board electronics[56–59,75,76,116–118] (Fig. 4(a)(left)). To hold the weight of the body, the SMA is typically embedded inside a polymer [58,59,61,76,116,117] or combined with a complex origami structure [116,119,120] that is externally attached to the rest of the body to increase the stiffness. During actuation, the SMA limbs switch between a curled/bent shape and less-curled/straight shape to exert force on the ground to propel the robot forward.[58,59,61,75,76,116,117] (Fig. 4(a)(left)). By integrating load-bearing SMA limbs, miniaturized batteries, and flexible electronics, Huang et al. developed compact, palm-sized SMA-driven soft robots that were untethered and approach the speed of natural organisms [58,61,75] (Fig. 4(a)(left)). With this implementation, they demonstrated that limbed SMA-driven soft crawling robots are capable of navigating through unstructured terrains and crawling over obstacles. Such capabilities expand the range of mobility that had been previously demonstrated with other SMA-driven soft robots[58,61,75]. Another type of SMA-driven soft crawling robot involves worm-like motion, which takes advantage of the strain change between martensite and austenite phase of nitinol (Fig. 4(a)(right)). SMA wire or springs are directly attached to a mesh-like[121] or silicone body [122–124] (Fig. 4(a)(right)) and the body changes length during crawling**.** Anisotropic features are commonly applied to the robot to achieve anisotropic friction. Although suffering from low locomotion speed, the worm-like design gives the robots robustness to resist high mechanical impact[118].

In addition to crawling, SMA-powered robots are also capable of mobility through rolling, climbing, and jumping. By exploiting rolling inertia, rolling robots can be designed to achieve faster locomotion speeds relative to crawling robots. For these implementations, the SMA generates rolling locomotion either by morphing the shape of the robot leading to the movement of the centre of mass [61,119,120,125,126] (Fig. 4(b)(left)) or by serving as a propulsion mechanism to propel the robot rolling forward [117](Fig. 4(b)(right)). Taking advantage of high strain output, high force-to-weight ratio, and low requirement of auxiliary equipment, SMAs have also been implemented as promising actuators on climbing robots that combine adhesion mechanisms such as electrostatic adhesion (Fig. 4(c)(left))[127], electromagnetic adhesion[128] and microspine arrays (Fig. 4(c)(right))[129]. Likewise, their high force-to-weight ratio makes SMAs well suited for jumping locomotion. Although tethered, the SMA-driven soft jumping robots presented in [119,125,130] and [61] utilize a pre-strained SMA wire (Fig. 4(d)(left)) and spring (Fig.4(d)(right)) respectively to achieve dramatic shape change in a short amount of time leading to a jumping motion. With the development of lightweight batteries and optimization of electronic design, SMAs have the potential to eventually be integrated into an untethered soft jumping system.

Swimming soft robots driven by SMA take advantage of convective cooling in water for fast cooling of the actuators to improve the actuation frequencies. Additionally, swimming soft robots driven by SMA have potential use in a wide range of applications, including fish farming, coastal protection, live animal monitoring and surveillance due to its silent actuation property[114,115]. In one implementation that mimics the caudal fin of fish, multiple SMAs were assigned symmetrically on both sides of the centreline to achieve bi-directional oscillation (Fig. 4(e)(left))[115]. SMA actuators have also been implemented in other soft robots inspired by aquatic organisms such as the frog[66] and jellyfish[131]. As in Ref. [57], Nitinol was embedded in thermal conductive elastomer in order to create limb-like flexural actuators that were used to propel a frog-inspired swimmer[66]. For the jellyfish-inspired robot, SMA spring was embedded inside the elastomer body of the robot to achieve a radial contraction leading to a downward and inward paddle locomotion to propel upward. A similar implementation of soft SMA actuators in a swimming robotic system presented in Coral et al.'s work used an SMA actuator as a valve to control the water volume in the swimmer by radial contraction, resulting in forward locomotion (Fig. 4(e)(right))[132].

As shown above, SMAs have been implemented in a variety of soft robots as actuation components to achieve varied locomotion including crawling, rolling, climbing, jumping and swimming. With the ultimate goal of building autonomous, fast-moving soft robots, future efforts could be directed towards embedded sensors that enable close-loop control as well as miniaturized on-board electronics to achieve untethered locomotion.

3.2 LCE-Powered Robots

Unlike SMAs, soft robots and soft robotic architectures that use Joule heated LCE actuators have been largely limited to micromachines[133,134] and useful but niche architectures, like an iris-like aperture (Fig. 5(a))[135]. Also common are swimmers and crawlers that use light to induce actuation[136]. Soft robots that use Joule heated LCE actuators might find application in areas where photoactuation is difficult or impossible. There has been recent progress in LCE-based soft robotics. Here, we review progress toward Joule heating in LCE-based soft robotics over the past few years.

Soft crawlers are common soft robotic architectures that have been attempted in recent works. Yuan et al. used a 3D printed structure and laminated an LCE actuator to form a soft robotic crawler that moved at 3 mm min^{-1}[110]. Similar rates were achieved for other crawlers that used bilayer or hinge structures[45,102,105]. Efforts to improve actuation speed require management of power and duty cycle.

The fastest crawler to date that used Joule heating LCEs moved at a rate of 44 mm min^{-1}[94], which is still >25 slower than the fastest SMA walkers. In this work, the authors used a bilayer structure of Kapton film along with a reprogrammable LCE for complex actuation. By selectively placing Kapton tape along the LCE, unique and complex motion could be achieved. For example, the bilayer actuator could be Joule-heated in a cylindrical tube and crawl through the tube. The LCE soft robotic architecture could generate motion that would push a weight (Fig. 5(b)).

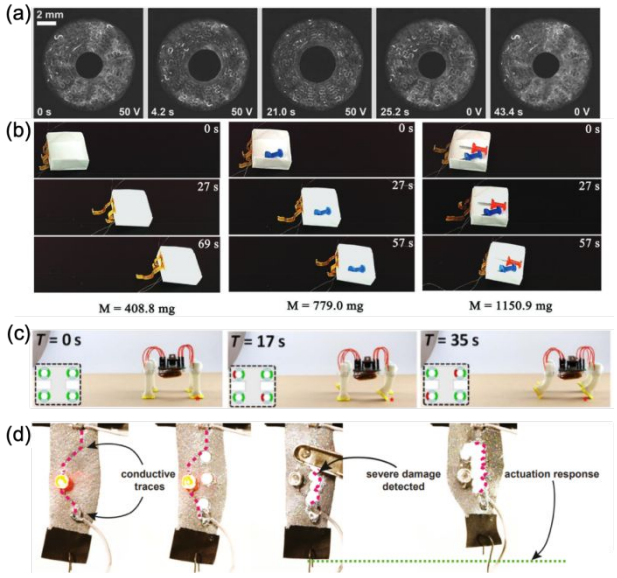

Fig. 5 LCEs have bene previously used for micromachines and other applications like an iris-like aperture (a) (Reproduced with permission, [135], 2014, Wiley). More recently, LCE actuators can be Joule-heated to form soft robotic architectures that can push a weight (b) (Reproduced with permission [94], 2019, Wiley). Further efforts toward robots that are untethered (c) and that can sense and respond to their environment (d) will be useful for the future of LCEs in soft robotics (Reproduced with permission [90], 2019, AAAS and [45], 2019, NAS).

Another example of a soft robotic implementation with LCEs used soft tubular actuators with multimodal actuation capabilities[90]. The tubular actuators were LCE sheets that were rolled, and wires for Joule heating were sandwiched between the sheets. The wires could be selectively heated for multimodal actuation. The multimodal actuation enabled simultaneous gripping and twisting motions for a soft gripper. The twisting motion could twist a cap on a vial. Multimodal actuation could also be used for a walking gait for a four-legged walker (Fig. 5(c)). The walker was untethered, using a microcontroller, MOSFETs, and a lithium polymer battery as the on-board power supply.

Future work should explore methods for sensing and control of soft robotics with LCEs[137]. In our recent work, we fabricated LCE actuators filled with droplets of a gallium-based liquid metal to improve thermal and electrical conductivity[45]. Since the composite was conductive, it could be paired with a microcontroller for touch sensing, and similar composites showed the capability of damage detection. We showed that the liquid metal-LCE actuator could also sense damage and even be designed to autonomously respond to damage (Fig. 5(d)). This damage sensing and response without the need for on-board sensors could be useful for soft robotics, but our current implementation was highly deterministic and only responded under carefully controlled conditions. Others have integrated sensors like photodetectors into crawling soft robots such that the robot was programmed to Joule heat certain regions in response to a signal from the photodetector[105]. The robot would crawl when green and red lights were switched on and off. Again, this response is a positive step forward towards soft robotics that use LCE actuators, but future research should strive to make responsiveness more representative of real-world conditions.

4 Other Shape Changing Materials

The shape memory materials discussed here represent just a small subset of materials that can be engineered to change shape in response to electrical stimulation. Dielectric elastomer actuators (DEAs) represent another popular class of electro-responsive shape changing materials. DEAs have been extensively covered in the literature, including several recent review papers that focus on their specific applications to soft robotics[138,139]. Another exciting area of research is in the emerging field of electro-responsive hydrogels. Hydrogels are 3D networks of hydrophilic polymer infiltrated with a high volume content of water or aqueous media that have biologically relevant softness[140], biocompatibility[141,142], bioactivity[142,143], and high hydrophilicity[144].

Electro-responsive hydrogel can be engineered to actuate when stimulated by an external electric field (~0.1-500 V/mm) [145–154]instead of Joule heating from direct current. The electric field results in a nonuniform distribution of ions that causes osmotic pressure imbalance, leading to a bending motion of the actuator. As a result, electro-responsive hydrogel actuators can require significantly less power consumption compared with SMA and LCE actuators. However, existing actuators are currently limited by low power density and are not able to match the high force density of SMAs[140,147,148,150,155].

Nonetheless, electro-responsive hydrogel actuators have been successfully **implemented into soft robotic systems to achieve varied functionalities such as soft grippers[149,155,156], biomimetic robots[153,154,156,157] and microfluidic devices[145,146,152,158–160]. Applications of** electro-responsive hydrogel actuators can be limited by low actuation speed, low actuation force, and dependency on an aqueous environment since they are driven by osmotic pressure induced swelling and deswelling in the aqueous solution. F**uture** work could focus on improving performance by synthesising electro-responsive hydrogels with higher response speed for fast moving robots. Developing novel material or structural architectures of hydrogels with additional functionalities such as sensing could also be beneficial for making untethered and autonomous soft robots.

5 Conclusions & Outlook

In this highlight article, we have presented progress over the past few years in developing soft robot actuators using shape memory materials. In particular, we have focused on Nitinol SMA and LCEs since these represent the popular shape memory materials for soft robot actuation. All classes of materials are

capable of reversible strains, force outputs, work densities, and activation speeds that are adequate for soft robot shape change and mobility. Although the shape memory response is primarily controlled by thermally-driven phase change, these actuators can be electrically activated. This electrical activation allows soft actuators with SMAs or LCEs to be operated in untethered soft robots using miniaturized, on-board batteries and circuitry.

Although promising for applications in soft robotics, SMA and LCE based soft actuators currently have certain disadvantages that limit their performance and applicability. SMA and LCE actuators suffer from low actuation frequencies and poor energy efficiency because they are thermally driven. These properties can result in slow locomotion speeds and short operational time on a single battery charge. Future efforts should address these challenges with novel materials chemistry, composite material architectures, and device-level materials integration that improve the speed of activation/deactivation and enable recovery of thermal energy. Such efforts could potentially leverage methods for computational design and modelling of shape memory materials as well as ongoing investments in 4D printing and stretchable electronics integration, enabling meaningful advancements in soft robotics.

Conflicts of interest

There are no conflicts to declare.

Acknowledgements

This material is based upon work supported in part by the US Army Research Office under Contract/Grants W911NF-18-1-0150 and W911NF-16-1-0148 (Program Manager: Dr. Samuel C. Stanton) and Office of Naval Research (ONR) under grant # N00014-17-1-2063 (Program Manager: Dr. Tom McKenna).

Notes and references

[1] C. Majidi, *Adv. Mater. Technol.* **2019**, *4*, 1800477.
[2] G. M. Whitesides, *Angew. Chemie - Int. Ed.* **2018**, *57*, 4258-4273.
[3] P. Polygerinos, N. Correll, S. A. Morin, B. Mosadegh, C. D. Onal, K. Petersen, M. Cianchetti, M. T. Tolley, R. F. Shepherd, *Adv. Eng. Mater.* **2017**, *19*, 1700016.
[4] D. Trivedi, C. D. Rahn, W. M. Kier, I. D. Walker, *Appl. Bionics Biomech.* **2008**, *5*, 99.
[5] F. Daerden, D. Lefeber, *Eur. J. Mech. Environ. Eng.* **2002**, *47*, 11-21.
[6] W. McMahan, V. Chitrakaran, M. Csencsits, D. Dawson, I. D. Walker, B. A. Jones, M. Pritts, D. Dienno, M. Grissom, C. D. Rahn, In *Proceedings - IEEE International Conference on Robotics and Automation*; 2006; p. 2336-2341.
[7] S. I. Rich, R. J. Wood, C. Majidi, *Nat. Electron.* **2018**, *1*, 102-112.
[8] J. Mohd Jani, M. Leary, A. Subic, M. A. Gibson, *Mater. Des.* **2014**, *56*, 1078-1113.
[9] L. Dong, Y. Zhao, *Mater. Chem. Front.* **2018**, *2*, 1932-1943.
[10] H. Finkelmann, Kock Hans-J., G. Rehage, *Die Makromol. Chemie, Rapid Commun.* **1981**, *2*, 317-322.
[11] T. J. White, D. J. Broer, *Nat. Mater.* **2015**, *14*, 1087-1098.
[12] R. S. Kularatne, H. Kim, J. M. Boothby, T. H. Ware, *J. Polym. Sci. Part B Polym. Phys.* **2017**, *55*, 395-411.
[13] L. Hines, K. Petersen, G. Z. Lum, M. Sitti, *Adv. Mater.* **2017**, *29*, 1603483.
[14] Q. Zhao, H. J. Qi, T. Xie, *Prog. Polym. Sci.* **2015**, *49-50*, 79-120.
[15] Y. Liu, H. Lv, X. Lan, J. Leng, S. Du, *Compos. Sci. Technol.* **2009**, *69*, 2064-2068.
[16] I. Chopra, *AIAA J.* **2002**, *40*, 2145-2187.
[17] O. Erol, A. Pantula, W. Liu, D. H. Gracias, *Adv. Mater. Technol.* **2019**, *4*, 1900043.
[18] C. Chluba, W. Ge, R. L. DeMiranda, J. Strobel, L. Kienle, E. Quandt, M. Wuttig, *Science (80-.).* **2015**, *348*, 1004-1007.
[19] J. Cui, Y. S. Chu, O. O. Famodu, Y. Furuya, J. Hattrick-Simpers, R. D. James, A. Ludwig, S. Thienhaus, M. Wuttig, Z. Zhang, I. Takeuchi, *Nat. Mater.* **2006**, *5*, 286-290.
[20] K. Hong, S. Lee, S. Han, Y. Yeon, *Appl. Sci.* **2018**, *8*, 730.
[21] M. Shahverdi, J. Michels, C. Czaderski, M. Motavalli, *Constr. Build. Mater.* **2018**, *173*, 586-599.
[22] R. Dasgupta, *J. Mater. Res.* **2014**, *29*, 1681-1698.
[23] J. Mohd Jani, M. Leary, A. Subic, *J. Intell. Mater. Syst. Struct.* **2017**, *28*, 1699-1718.
[24] B. Panton, Y. N. Zhou, M. I. Khan, *Smart Mater. Struct.* **2016**, *25*, 095027.
[25] P. Boyraz, G. Runge, A. Raatz, *Actuators* **2018**, *7*, 48.
[26] M. Shayan, N. Gildener-Leapman, M. Elsisy, J. T. Hastings, S. Kwon, W. H. Yeo, J. H. Kim, P. Shridhar, G. Salazar, Y. Chun, *Materials (Basel).* **2019**, *12*, 3555.
[27] S. V. Ahir, A. R. Tajbakhsh, E. M. Terentjev, *Adv. Funct. Mater.* **2006**, *16*, 556-560.
[28] M. O. Saed, A. H. Torbati, C. A. Starr, R. Visvanathan, N. A. Clark, C. M. Yakacki, *J. Polym. Sci. Part B Polym. Phys.* **2017**, *55*, 157-168.
[29] H. Wermter, H. Finkelmann, *E-Polymers* **2001**, *1*, 2197-4586.
[30] C. P. Ambulo, J. J. Burroughs, J. M. Boothby, H. Kim, M. R. Shankar, T. H. Ware, *ACS Appl. Mater. Interfaces* **2017**, *9*, 37332-37339.
[31] M. López-Valdeolivas, D. Liu, D. J. Broer, C. Sánchez-Somolinos, *Macromol. Rapid Commun.* **2018**, *39*, 1700710.
[32] A. Kotikian, R. L. Truby, J. W. Boley, T. J. White, J. A. Lewis, *Adv. Mater.* **2018**, *30*, 1706164.
[33] Z. Wang, Q. He, Y. Wang, S. Cai, *Soft Matter* **2019**, *15*, 2811-2816.
[34] J. Küpfer, H. Finkelmann, *Die Makromol. Chemie, Rapid Commun.* **1991**, *12*, 717-726.
[35] I. Kundler, H. Finkelmann, *Macromol. Rapid Commun.* **1995**, *16*, 679-686.
[36] T. H. Ware, M. E. McConney, J. J. Wie, V. P. Tondiglia, T. J. White, *Science (80-.).* **2015**, *347*, 982-984.
[37] A. Lendlein, O. E. C. Gould, *Nat. Rev. Mater.* **2019**, *4*, 116.
[38] Z. S. Davidson, H. Shahsavan, A. Aghakhani, Y. Guo, L. Hines, Y. Xia, S. Yang, M. Sitti, *Sci. Adv.* **2019**, *5*, eaay0855.
[39] A. Jákli, *Liq. Cryst.* **2010**, *37*, 825-837.
[40] W. Lehmann, H. Skupin, C. Tolksdorf, E. Gebhard, R. Zentel, P. Krüger, M. Lösche, F. Kremer, *Nature* **2001**, *410*, 447-450.
[41] C. Huang, Q. Zhang, A. Jákli, *Adv. Funct. Mater.* **2003**, *13*, 525-529.
[42] C. M. Spillmann, J. Naciri, B. D. Martin, W. Farahat, H. Herr, B. R. Ratna, *Sensors Actuators, A Phys.* **2007**, *133*, 500-505.

[43] M. Chambers, B. Zalar, M. Remškar, S. Žumer, H. Finkelmann, *Appl. Phys. Lett.* **2006**, *89*, 243116.
[44] A. Agrawal, H. Chen, H. Kim, B. Zhu, O. Adetiba, A. Miranda, A. Cristian Chipara, P. M. Ajayan, J. G. Jacot, R. Verduzco, *ACS Macro Lett.* **2016**, *5*, 1386-1390.
[45] M. J. Ford, C. P. Ambulo, T. A. Kent, E. J. Markvicka, C. Pan, J. Malen, T. H. Ware, C. Majidi, *Proc. Natl. Acad. Sci. U. S. A.* **2019**, *116*, 21438-21444.
[46] S. Barbarino, E. L. Saavedra Flores, R. M. Ajaj, I. Dayyani, M. I. Friswell, *Smart Mater. Struct.* **2014**, *23*, 063001.
[47] A. J. Taylor, T. Slutzky, L. Feuerman, H. Ren, J. Tokuda, K. Nilsson, Z. T. H. Tse, *IEEE/ASME Trans. Mechatronics* **2019**, *24*, 883-888.
[48] Y. Zhang, M. Su, M. Li, R. Xie, H. Zhu, Y. Guan, In *2017 IEEE International Conference on Mechatronics and Automation, ICMA*; 2017; p. 677-682.
[49] H. Yang, M. Xu, W. Li, S. Zhang, *IEEE Trans. Ind. Electron.* **2019**, *66*, 6108-6116.
[50] S. S. Cheng, Y. Kim, J. P. Desai, *J. Intell. Mater. Syst. Struct.* **2017**, *28*, 2167-2183.
[51] M. Boyvat, J. S. Koh, R. J. Wood, *Sci. Robot.* **2017**, *2*, 1-10.
[52] A. I. Nawroj, A. M. Dollar, *IEEE Robot. Autom. Lett.* **2017**, *2*, 1878-1884.
[53] Y. Zhang, H. Ren, In *IEEE International Conference on Robotics and Biomimetics (ROBIO)*; 2019; p. 1338-1343.
[54] S. M. An, J. Ryu, M. Cho, K. J. Cho, *Smart Mater. Struct.* **2012**, *21*, 055009.
[55] C. H. Park, K. J. Choi, Y. S. Son, *IEEE/ASME Trans. Mechatronics* **2019**, *24*, 1798-1807.
[56] M. D. Bartlett, N. Kazem, M. J. Powell-Palm, X. Huang, W. Sun, J. A. Malen, C. Majidi, *Proc. Natl. Acad. Sci. U. S. A.* **2017**, *114*, 2143-2148.
[57] X. Huang, K. Kumar, K. M. Jawed, A. M. Nasab, Z. Ye, W. Shan, C. Majidi, *Adv. Mater. Technol.* **2019**, *4*, 1800540.
[58] X. Huang, K. Kumar, K. M. Jawed, Z. Ye, C. Majidi, *IEEE Robot. Autom. Lett.* **2019**, *4*, 2415-2422.
[59] E. J. Markvicka, M. D. Bartlett, X. Huang, C. Majidi, *Nat. Mater.* **2018**, *17*, 618-624.
[60] M. Sivaperuman Kalairaj, H. Banerjee, C. M. Lim, P. Y. Chen, H. Ren, *RSC Adv.* **2019**, *9*, 34244-34255.
[61] X. Huang, K. Kumar, M. K. Jawed, A. M. Nasab, Z. Ye, W. Shan, C. Majidi, *Sci. Robot.* **2018**, *3*, eaau7557.
[62] H. Yuan, F. Chapelle, J. C. Fauroux, X. Balandraud, *Smart Mater. Struct.* **2018**, *27*, 055005.
[63] H. Rodrigue, W. Wang, D. R. Kim, S. H. Ahn, *Compos. Struct.* **2017**, *176*, 398-406.
[64] G. Chernyshov, F. Cao, B. Tag, G. Liu, C. Caremel, K. Kunze, In *Proceedings - International Symposium on Wearable Computers, ISWC*; 2018; p. 112-119.
[65] W. Wang, S. H. Ahn, In *2018 IEEE International Conference on Soft Robotics, RoboSoft 2018*; IEEE, 2018; p. 222-227.
[66] X. Huang, Z. Ren, C. Majidi, In *IEEE International Conference on Soft Robotics*; 2020.
[67] D. Cosovanu, D. Mândru, *ACTA Tech. NAPOCENSIS Ser. Appl. Math. Mech. Eng.* **2017**, *60*, 313-318.
[68] C. Xiang, J. Guo, Y. Chen, L. Hao, S. Davis, *IEEE Access* **2018**, *6*, 27183-27189.
[69] W. Wang, S. H. Ahn, *Soft Robot.* **2017**, *4*, 379-389.
[70] S. Akbari, A. H. Sakhaei, S. Panjwani, K. Kowsari, A. Serjourei, Q. Ge, *Sensors Actuators, A Phys.* **2019**, *290*, 177-189.
[71] M. W. Han, S. H. Ahn, *Adv. Mater.* **2017**, *29*, 1-6.
[72] H. Yin, J. Zhou, J. Li, V. S. Joseph, *J. Mater. Eng. Perform.* **2018**, *27*, 3581-3589.
[73] K. Eschen, J. Abel, *Smart Mater. Struct.* **2019**, *28*, 025014.
[74] X. Kong, H. Jin, Y. Chen, J. Yang, E. Dong, *2018 IEEE Int. Conf. Robot. Biomimetics, ROBIO* **2018**, 1202-1207.
[75] N. N. Goldberg, X. Huang, C. Majidi, A. Novelia, O. M. O'Reilly, D. A. Paley, W. L. Scott, *Soft Robot.* **2018**, *6*, 595-610.
[76] C. Liu, E. Dong, M. Xu, G. Alici, J. Yang, *Int. J. Adv. Robot. Syst.* **2018**, *15*, 1-14.
[77] N. Nayakanti, S. H. Tawfick, A. J. Hart, *Extrem. Mech. Lett.* **2018**, *21*, 17-24.
[78] M. Garces-Schroder, T. Zimmermann, C. Siemers, M. Leester-Schadel, M. Bol, A. Dietzel, *J. Microelectromechanical Syst.* **2019**, *28*, 869-881.
[79] M. C. Yuen, R. A. Bilodeau, R. K. Kramer, *IEEE Robot. Autom. Lett.* **2016**, *1*, 708-715.
[80] T. Liao, Z. T. H. Tse, H. Ren, In *IEEE/ASME International Conference on Advanced Intelligent Mechatronics, AIM*; 2019; p. 108-113.
[81] S. I. Rich, V. Nambeesan, R. Khan, C. Majidi, *J. Intell. Mater. Syst. Struct.* **2019**, *30*, 2908-2918.
[82] M. O. Saed, C. P. Ambulo, H. Kim, R. De, V. Raval, K. Searles, D. A. Siddiqui, J. M. O. Cue, M. C. Stefan, M. R. Shankar, T. H. Ware, *Adv. Funct. Mater.* **2019**, *29*, 1806412.
[83] M. Warner, M. E. Terentjev, *Liquid Crystal Elastomers*; 2007.
[84] Z. Pei, Y. Yang, Q. Chen, E. M. Terentjev, Y. Wei, Y. Ji, *Nat. Mater.* **2014**, *13*, 36-41.
[85] C. M. Yakacki, M. Saed, D. P. Nair, T. Gong, S. M. Reed, C. N. Bowman, *RSC Adv.* **2015**, *5*, 18997-19001.
[86] M. O. Saed, A. H. Torbati, D. P. Nair, C. M. Yakacki, *J. Vis. Exp.* **2016**, *107*, e53546.
[87] Y. Ji, J. E. Marshall, E. M. Terentjev, *Polymers (Basel).* **2012**, *4*, 316-340.
[88] H. Kim, J. M. Boothby, S. Ramachandran, C. D. Lee, T. H. Ware, *Macromolecules* **2017**, *50*, 4267-4275.
[89] H. F. Lu, M. Wang, X. M. Chen, B. P. Lin, H. Yang, *J. Am. Chem. Soc.* **2019**, *141*, 14364-14369.
[90] Q. He, Z. Wang, Y. Wang, A. Minori, M. T. Tolley, S. Cai, *Sci. Adv.* **2019**, *5*, eaax5746.
[91] Y. Y. Huang, J. Biggins, Y. Ji, E. M. Terentjev, *J. Appl. Phys.* **2010**, *107*, 083515.
[92] N. Torras, M. Duque, C. J. Camargo, J. Esteve, A. Sánchez-Ferrer, *Soft Matter* **2017**, *13*, 7264-7272.
[93] C. Feng, C. P. H. Rajapaksha, J. M. Cedillo, C. Piedrahita, J. Cao, V. Kaphle, B. Lüssem, T. Kyu, A. Jákli, *Macromol. Rapid Commun.* **2019**, *40*, 1900299.
[94] Y. Y. Xiao, Z. C. Jiang, X. Tong, Y. Zhao, *Adv. Mater.* **2019**, *31*, 1903452.
[95] H. Aharoni, Y. Xia, X. Zhang, R. D. Kamien, S. Yang, *Proc. Natl. Acad. Sci. U. S. A.* **2018**, *115*, 7206-7211.
[96] M. Barnes, R. Verduzco, *Soft Matter* **2019**, *15*, 870-879.
[97] A. Buguin, M. H. Li, P. Silberzan, B. Ladoux, P. Keller, *J. Am. Chem. Soc.* **2006**, *128*, 1088-1089.
[98] M. Tabrizi, T. H. Ware, M. R. Shankar, *ACS Appl. Mater. Interfaces* **2019**, *11*, 28236-28245.
[99] Y. Yao, J. T. Waters, A. V. Shneidman, J. Cui, X. Wang, N. K. Mandsberg, S. Li, A. C. Balazs, J. Aizenberg, *Proc. Natl. Acad. Sci. U. S. A.* **2018**, *115*, 12950-12955.
[100] J. Naciri, A. Srinivasan, H. Jeon, N. Nikolov, P. Keller, B. R. Ratna, *Macromolecules* **2003**, *36*, 8499-8505.

[101] D. J. Roach, C. Yuan, X. Kuang, V. C. F. Li, P. Blake, M. L. Romero, I. Hammel, K. Yu, H. J. Qi, *ACS Appl. Mater. Interfaces* **2019**, *11*, 19514-19521.

[102] A. Minori, S. Jadhav, Q. He, S. Cai, M. T. Tolley, In *ASME 2017 Conference on Smart Materials, Adaptive Structures and Intelligent Systems, SMASIS*; 2017.

[103] M. Shahinpoor, In *Smart Structures and Materials 2000: Electroactive Polymer Actuators and Devices (EAPAD)*; 2000; p. 187-192.

[104] C. Ohm, M. Brehmer, R. Zentel, In *Adv Polym Sci*; 2012; pp. 49–93.

[105] C. Wang, K. Sim, J. Chen, H. Kim, Z. Rao, Y. Li, W. Chen, J. Song, R. Verduzco, C. Yu, *Adv. Mater.* **2018**, *30*, 1706695.

[106] J. Hong, D. W. Park, S. E. Shim, *Macromol. Res.* **2012**, *20*, 465-472.

[107] H. Kim, J. A. Lee, C. P. Ambulo, H. B. Lee, S. H. Kim, V. V. Naik, C. S. Haines, A. E. Aliev, R. Ovalle-Robles, R. H. Baughman, T. H. Ware, *Adv. Funct. Mater.* **2019**, *29*, 1905063.

[108] S. Courty, J. Mine, A. R. Tajbakhsh, E. M. Terentjev, *Europhys. Lett.* **2003**, *64*, 654-660.

[109] T. Guin, B. A. Kowalski, R. Rao, A. D. Auguste, C. A. Grabowski, P. F. Lloyd, V. P. Tondiglia, B. Maruyama, R. A. Vaia, T. J. White, *ACS Appl. Mater. Interfaces* **2018**, *10*, 1187-1194.

[110] C. Yuan, D. J. Roach, C. K. Dunn, Q. Mu, X. Kuang, C. M. Yakacki, T. J. Wang, K. Yu, H. J. Qi, *Soft Matter* **2017**, *13*, 558-5568.

[111] D. J. Roach, X. Kuang, C. Yuan, K. Chen, H. J. Qi, *Smart Mater. Struct.* **2018**, *27*, 125011.

[112] A. Kotikian, C. McMahan, E. C. Davidson, J. M. Muhammad, R. D. Weeks, C. Daraio, J. A. Lewis, *Sci. Robot.* **2019**, *4*, eaax7044.

[113] K. Institut, **2018**, 25-27.

[114] Y. Tadesse, A. Villanueva, C. Haines, D. Novitski, R. Baughman, S. Priya, *Smart Mater. Struct.* **2012**, *21*, 045013.

[115] W. Coral, C. Rossi, O. M. Curet, D. Castro, *Bioinspiration and Biomimetics* **2018**, *13*, 056009.

[116] D. Lee, K. Saito, T. Umedachi, T. D. Ta, Y. Kawahara, *UbiComp/ISWC 2018 - Adjun. Proc. 2018 ACM Int. Jt. Conf. Pervasive Ubiquitous Comput. Proc. 2018 ACM Int. Symp. Wearable Comput.* **2018**, 392-395.

[117] J. Pan, Z. Shi, T. Wang, *Sci. China Technol. Sci.* **2019**, *62*, 1401-1411.

[118] S. Seok, C. D. Onal, R. Wood, D. Rus, S. Kim, In *Proceedings - IEEE International Conference on Robotics and Automation*; 2010; p. 1228-1233.

[119] Z. Zhakypov, C. H. Belke, J. Paik, In *IEEE International Conference on Intelligent Robots and Systems*; 2017; p. 5580-5586.

[120] L. M. Fonseca, G. V. Rodrigues, M. A. Savi, A. Paiva, *Chaos, Solitons and Fractals* **2019**, *122*, 245-261.

[121] R. Patil, N. Patra, A. Sharma, P. Kavitha, I. Apalani, *IOP Conf. Ser. Mater. Sci. Eng.* **2018**, *390*, 012044.

[122] T. Umedachi, Y. Kawahara, In *2018 IEEE International Conference on Soft Robotics, RoboSoft*; IEEE, 2018; p. 461-466.

[123] J. O. Alcaide, L. Pearson, M. E. Rentschler, In *Proceedings - IEEE International Conference on Robotics and Automation*; IEEE, 2017; p. 4338-4345.

[124] S. Chatterjee, R. Niiyama, Y. Kawahara, In *2017 IEEE International Conference on Robotics and Biomimetics, ROBIO 2017*; 2017; p. 1-6.

[125] Y. S. Chung, J.-H. Lee, J. H. Jang, H. R. Choi, H. Rodrigue, *ACS Appl. Mater. Interfaces* **2019**, *11*, 40793-40799.

[126] J. L. Kennedy, A. K. Fontecchio, In *2017 3rd International Conference on Control, Automation and Robotics, ICCAR*; IEEE, 2017; p. 237-241.

[127] Q. Wu, V. Pradeep, X. Liu, *2018 IEEE Int. Conf. Soft Robot. RoboSoft 2018* **2018**, 315-320.

[128] J. Li, W. Chang, Q. Li, *Smart Mater. Struct.* **2018**, *27*, 115020.

[129] Q. Hu, E. Dong, G. Cheng, H. Jin, J. Yang, D. Sun, In *IEEE International Conference on Intelligent Robots and Systems*; 2019; p. 5800-5805.

[130] Z. Ren, H. Wang, W. Chen, In *2017 IEEE International Conference on Robotics and Biomimetics, ROBIO*; 2018; p. 605-610.

[131] M. A. Kazemi Lari, A. D. Dostine, J. Zhang, A. S. Wineman, J. A. Shaw, In *Proc. SPIE 10965, Bioinspiration, Biomimetics, and Bioreplication IX*; 2019; p. 1096504.

[132] S. Guo, S. Sun, J. Guo, In *2017 IEEE International Conference on Mechatronics and Automation, ICMA*; 2017; p. 1314-1319.

[133] A. Sánchez-Ferrer, T. Fischl, M. Stubenrauch, H. Wurmus, M. Hoffmann, H. Finkelmann, *Macromol. Chem. Phys.* **2009**, *210*, 1671-1677.

[134] A. Sánchez-Ferrer, T. Fischl, M. Stubenrauch, A. Albrecht, H. Wurmus, M. Hoffmann, H. Finkelmann, *Adv. Mater.* **2011**, *23*, 4526-4530.

[135] S. Schuhladen, F. Preller, R. Rix, S. Petsch, R. Zentel, H. Zappe, *Adv. Mater.* **2014**, *26*, 7247-7251.

[136] H. Zeng, O. M. Wani, P. Wasylczyk, A. Priimagi, *Macromol. Rapid Commun.* **2018**, *39*, 1700224.

[137] S. Petsch, R. Rix, B. Khatri, S. Schuhladen, P. Müller, R. Zentel, H. Zappe, *Sensors Actuators, A Phys.* **2015**, *15*, 44-51.

[138] U. Gupta, L. Qin, Y. Wang, H. Godaba, J. Zhu, *Smart Mater. Struct.* **2019**, *28*, 103002.

[139] J. H. Youn, S. M. Jeong, G. Hwang, H. Kim, K. Hyeon, J. Park, K. U. Kyung, *Appl. Sci.* **2020**, *10*, 640.

[140] P. Calvert, *Adv. Mater.* **2009**, *21*, 743-756.

[141] N. Huebsch, E. Lippens, K. Lee, M. Mehta, S. T. Koshy, M. C. Darnell, R. M. Desai, C. M. Madl, M. Xu, X. Zhao, O. Chaudhuri, C. Verbeke, W. S. Kim, K. Alim, A. Mammoto, D. E. Ingber, G. N. Duda, D. J. Mooney, *Nat. Mater.* **2015**, *14*, 1269-1277.

[142] J. Su, B.-H. Hu, W. L. Lowe, D. B. Kaufman, P. B. Messersmith, *Biomaterials* **2010**, *31*, 308-314.

[143] M. W. Tibbitt, K. S. Anseth, *Biotechnol. Bioeng.* **2009**, *103*, 655-663.

[144] J. Li, D. J. Mooney, *Nat. Rev. Mater.* **2016**, *1*, 16071.

[145] L. Engel, C. Liu, N. M. Hemed, Y. Khan, A. C. Arias, Y. Shacham-Diamand, S. Krylov, L. Lin, *J. Micromechanics Microengineering* **2018**, *28*, 105005.

[146] M. J. Bassetti, A. N. Chatterjee, N. R. Aluru, D. J. Beebe, *J. Microelectromechanical Syst.* **2005**, *14*, 1198-1207.

[147] T. Tungkavet, N. Seetapan, D. Pattavarakorn, A. Sirivat, *Mater. Sci. Eng. C* **2015**, *46*, 281-289.

[148] W. Sangwan, K. Petcharoen, N. Paradee, W. Lerdwijitjarud, A. Sirivat, *Carbohydr. Polym.* **2016**, *151*, 213-222.

[149] E. Palleau, D. Morales, M. D. Dickey, O. D. Velev, *Nat. Commun.* **2013**, *4*, 2257.
[150] T. Srisawasdi, K. Petcharoen, A. Sirivat, A. M. Jamieson, *Mater. Sci. Eng. C* **2015**, *56*, 1-8.
[151] M. L. O'Grady, P. Kuo, K. K. Parker, *ACS Appl. Mater. Interfaces* **2010**, *2*, 343-346.
[152] E. A. Moschou, S. F. Peteu, L. G. Bachas, M. J. Madou, S. Daunert, *Chem. Mater.* **2004**, *16*, 2499-2502.
[153] C. Yang, W. Wang, C. Yao, R. Xie, X.-J. Ju, Z. Liu, L.-Y. Chu, *Sci. Rep.* **2015**, *5*, 13622.
[154] D. Morales, E. Palleau, M. D. Dickey, O. D. Velev, *Soft Matter* **2014**, *10*, 1337-1348.
[155] C. Yang, Z. Liu, C. Chen, K. Shi, L. Zhang, X.-J. Ju, W. Wang, R. Xie, L.-Y. Chu, *ACS Appl. Mater. Interfaces* **2017**, *9*, 15758-15767.
[156] D. Han, C. Farino, C. Yang, T. Scott, D. Browe, W. Choi, J. W. Freeman, H. Lee, *ACS Appl. Mater. Interfaces* **2018**, *10*, 17512-17518.
[157] G. H. Kwon, J. Y. Park, J. Y. Kim, M. L. Frisk, D. J. Beebe, S.-H. Lee, *Small* **2008**, *4*, 2148-2153.
[158] T. Guan, F. Godts, F. Ceyssens, E. Vanderleyden, K. Adesanya, P. Dubruel, H. P. Neves, R. Puers, *Sensors Actuators A Phys.* **2012**, *186*, 184-190.
[159] G. H. Kwon, G. S. Jeong, J. Y. Park, J. H. Moon, S.-H. Lee, *Lab Chip* **2011**, *11*, 2910-2915.
[160] G. H. Kwon, Y. Y. Choi, J. Y. Park, D. H. Woo, K. B. Lee, J. H. Kim, S.-H. Lee, *Lab Chip* **2010**, *10*, 1604-1610.